Research Article

Biological evaluation, molecular docking and DFT calculations of pyrrole-based derivatives as dual acting AChE/MAO-B inhibitors

Emilio Mateev[1], Maya Georgieva[1]

1 *Department of Pharmaceutical Chemistry, Faculty of Pharmacy, Medical University-Sofia, Sofia, Bulgaria*

Corresponding author: Emilio Mateev (e.mateev@pharmfac.mu-sofia.bg)

Citation: Mateev E, Georgieva M (2023) Biological evaluation, molecular docking and DFT calculations of pyrrole-based derivatives as dual acting AChE/MAO-B inhibitors. Pharmacia 70(4): 1019–1026. https://doi.org/10.3897/pharmacia.70.e113014

Abstract

Considering the complex pathophysiology of Alzheimer's disease (AD), the multitarget ligand strategy is expected to provide superior effects for the treatment of the neurological disease compared to the classic single target strategy. Thus, six pyrrole-based compounds were evaluated for their dual monoamine oxidase type B (MAO-B) and acetylcholinesterase (AChE) inhibitory capacities. Most of the compounds revealed good AChE activities at 10 µM concentrations. 5d most potently inhibited AChE with 75%, while the hydrazide 5 demonstrated blocking effect of 51% at 10 µM concentrations. However, limited MAO-B inhibitory effects were observed with the exception of compounds 3, and especially 5 (30% inhibition at 1 µM). The *in vitro* assessments showed that the unsubstituted pyrrole-based hydrazide 5 is the best dual inhibitor of MAO-B/AChE enzymes. Subsequent *in silico* molecular docking simulations of 5 in the active sites of MAO-B (2V5Z) and AChE (4EY6) displayed the formation of stable enzyme-ligand complexes. To rationalize the biological assays, density functional theory (DFT) calculations were carried out at the B3LYP/6-311^{++}(d,p) level of theory. Overall, the results demonstrated that the pyrrole-based hydrazide 5 is a dual-acting AchE/MAO-B inhibitor with good antioxidant properties, which could be considered as a candidate for future lead-optimizations.

Keywords

Introduction

Alzheimer's disease (AD) is a neurodegenerative disorder with a chronic, and progressive character which accounts for more than half of the dementia cases (Huang et al. 2020). As the most common neurological disease, constant efforts are invested into the design and synthesis of novel anti-AD molecules (Mathew et al. 2019). Recently, therapies including monoclonal antibodies are of huge interest considering the direct aim towards the amyloid-based hypothesis. However, the high price of the
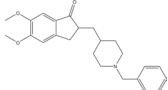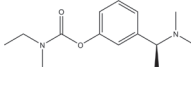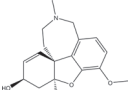
therapeutic courses, the need for frequent monitoring, as well as the questions about the overall efficacy of the monoclonal approaches have been discussed (Karlawish and Grill 2021; Tanzi 2021). Therefore, the symptomatic approach against AD is the main option of treatment.

The role of acetylcholine in the recovery of cognitive processes is known from decades. Pharmacologically active drugs acting as acetylcholinesterase (AChE) inhibitors are frequently employed for patients suffering from AD (Sitaram et al. 1978). Drugs such as Donepezil, Ri-

PENSOFT.

vastigmine and Galantamine are registered as AChE inhibitors (Raina et al. 2008) (Table 1).

Donepezil (IUPAC: (RS)-2-[(1-Benzyl-4-piper-

Table 1. Registered AChE inhibitors.

| Donepezil | Rivastigmine | Galantamine |

idyl)methyl]-5,6-dimethoxy-2,3-dihydroinden-1-one) is approved for the treatment of AD in more than 90 countries. It was first approved in 1996. Rivastigmine (IUPAC: (S)-3-[1-(dimethylamino)ethyl]phenyl N-ethyl-N-methylcarbamate) was accepted for the AD treatment a year after the approval of Donepezil. Galantamine (IUPAC: (1S,12S,14R)-9-methoxy-4-methyl-11-oxa-4-azatetracyclo[8.6.1.0^{1,12}.0^{6,17}]heptadeca-6(17),7,9,15-tetraen-14-ol was isolated from *Galanthus woronowii* and registered in 2000 for the treatment of AD (Galimberti and Scarpini 2016). Moreover, the interest of the discovery of novel MAO-B inhibitors was reignited considering the role of MAO-B in the pathophysiology of AD. (Schedin-Weiss et al. 2017). Molecules with a pyrrol moiety are frequently introduced as novel pharmacologycaly active drugs (Mateev et al. 2022b). Moreover, several articles have reported excellent AChE and MAO-B inhibitory effects of compounds comprising hydrazide or hydrazide-hydrazones motifs (Mohsen et al. 2015; Mateeva et al. 2021; Popiołek 2021). Considering the complicated pathophysiology of AD, most recent works have been focused on the search for novel multitarget ligands with effects against multiple enzymes (MAO-B/AChE) (Raka et al. 2020).

The main target of this study was to investigate the MAO-B and AChE inhibitory activities of recently obtained hydrazide-hydrazones through *in vitro* and *in silico* studies. The title compounds were compared with standard MAO-B and AChE inhibitors. Furthermore, molecular docking studies revealed the intermolecular interactions between the enzymes and the most prominent pyrrole-based dual inhibitor. An optimal geometric structure and frontier molecular orbital values of the most prominent dual acting MAO-B/AChE inhibitor were achieved through DFT simulations.

Materials and methods

Biological evaluations

In vitro MAO-B assay

The MAO-B effects were tested on a recombinant human MAO-B employing the fluorimetric method Amplex UltraRed reagent with several modifications (Mateev et al.

2022a). Tyramine hydrochloride was utilized as a substrate, and Selegiline as a positive control.

In vitro AChE assay

The AChE inhibitory effects of the title compounds were measured according to a modified Ellman's method (Chigurupati et al. 2016). Stock solutions (1 mg/ml) of the title compounds were diluted in DMSO. Subsequently, working solutions (concentrations of 10 μM) were prepared by serial dilutions. The test compounds (10 μM) were incubated with sodium phosphate buffer (0.1 M; pH 8.0; 200 μL), and AChE solution (0.1 U/mL; 40 μL) for 10 min at 36.5 °C. The reaction was initiated by addition of 5,5'-Dithiobis(2-nitrobenzoic acid (DTNB) (10 mM; 20 μL) and acetylthiocholine iodide (ATChI) (14 mM; 20 μL). The absorbance was measured using a microplate reader at 412 nm wavelength against a blank DMSO probe. The % inhibition was calculated against blank probes. Donepezil was applied as a positive control.

Molecular docking

The crystallographic structures of MAO-B (PDB: 2V5Z) and AChE (PDB: 4EY6) were retrieved from the Protein Data Bank (PDB). The initial protein structures of the target enzymes were refined with the Protein Preparation module in Maestro. Applying the former, hydrogen bonds were added, het states were generated and the crystallographic structures were minimized with the OPLS4 force field. The docking simulations were carried out with two robust docking softwares - GOLD 5.3 and Glide (Schrödinger Maestro Suite). The grid boxes were arranged around each co-crystallized ligand (Safinamide for MAO-B, and Galanthamine for AChE). Induced-fit docking (IFD) (Schrödinger) was used to enhance the robustness of the active conformations. The IFD enables full side chain flexibility and scores each new active solution with the Glide's XP score.

DFT calculations

All of the theoretical computations were carried out with Jaguar (Schrödinger Release 2022-1: Jaguar, Schrödinger, LLC, New York, NY, 2021.) (Bochevarov et al. 2013). Initially, the geometries of the most potent multitarget drugs were refined with conformational simulations with 250 iterations and OPLS4 force field. Subsequently, DFT calculations with Becke's three-parameter hybrid exchange–correlation functional (B3LYP) and 6-311^{++}G (d,p) basis set were performed. The frontier molecular orbitals (FMO) and the global reactivity descriptors for the most prominent drug were calculated at the same level of theory. The computational simulations were performed on an AMD Ryzen 9 5950X 16 core CPU and 64 GB of installed RAM. Windows 10 Pro was used as an operating system.

Results and discussion

Chemistry

The synthetic route of the title pyrrole-based derivatives was recently reported (Mateev et al. 2022a). One novel carboxylic acid 3, its corresponding hydrazide 5 and four new hydrazide-hydrazones 5a-d were obtained through Paal-Knorr condensation, hydrazide formation and condensations with various aldehydes, respectively (Fig. 1).
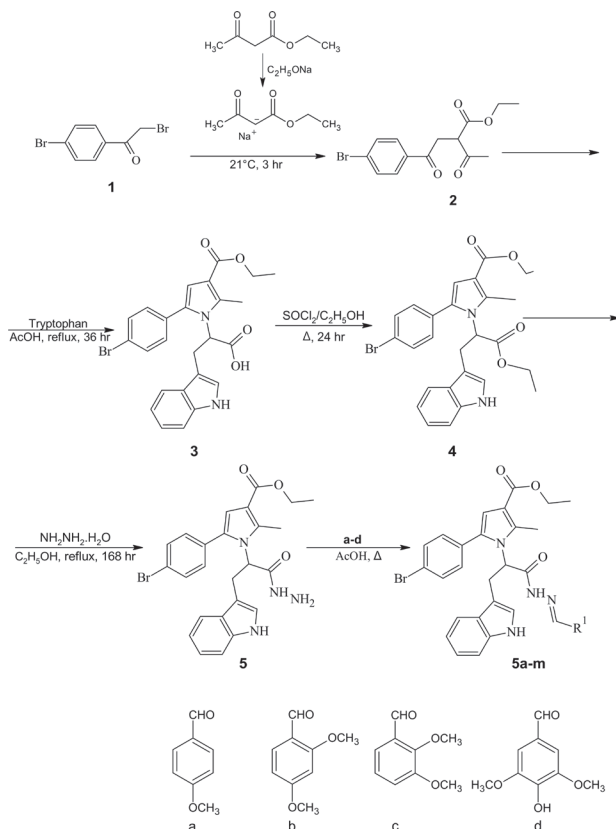

Figure 1. Synthetic route of the applied pyrrole-based hydrazide-hydrazones. All compounds were fully elucidated by instrumental (^{1}H NMR, FT-IR, and HRMS), and chromatographic analyses.

In vitro evaluations

Considering the complex pathophysiology of AD, numerous research groups emphasize on the design of multitarget drugs. The paradigm of one drug inhibiting multiple targets in the treatment of AD has successfully allowed the researchers to aim at several pathological components simultaneously (Gonzalez et al. 2019; Sang et al. 2022). Thus, the aforementioned tryptophan-comprising compounds were tested for their MAO-B and AChE inhibiting capacitates through *in vitro* assays.

In vitro MAO-B assay

Compounds 3, 5 and 5a-5d were screened for their MAO-B inhibitory activity by an *in vitro* fluorometric method. Selegiline was used as a standard drug. The results are given in Fig. 2.
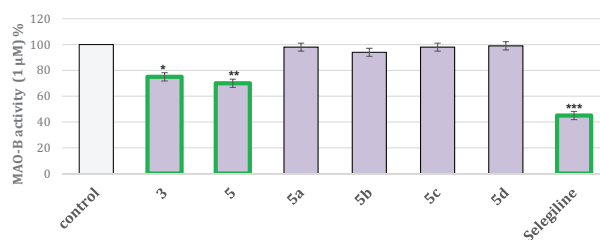

Figure 2. Activities of the title compounds against MAO-B applied as 1 μM concentrations. Data are presented as means from three independent experiments ± SD. * $P < 0.1$, ** $P < 0.01$, *** $P < 0.001$ vs control (pure hMAO-B).

The standard Selegiline demonstrated 55% hMAOB activity, compared to the control (pure hMAOB). The unsubstituted hydrazide 5 revealed a good inhibitory capacity of 30%, while the pyrrole acid (3) showed moderate activity of 25%. All hydrazide-hydrazones exerted no MAO-B inhibitory potential. Recent study held by Altintop et al. discussed the synthesis and evaluation of MAO-B effects of novel pyrrole-based compounds (Altintop et al. 2018). The most promising ligand displayed IC_{50} of 1.642 ± 0.082 μM. The molecular weights of the compounds varied in the range of 290–350 g/mol, which is significantly lower compared to the employed in this study dataset. Thus, further optimizations of the title pyrroles could be pointed towards lowering the molecular weights of the hydrazide-hydrazones.

In vitro AChE assay

The inhibitory capacity of the title compounds against eeAChE (electric eel acetylcholinesterase) was measured according to a modified Ellman's method (Chigurupati et al. 2016). Donepezil was used as a reference compound. The blocking capacities of the test compounds, at 10 μM concentrations, are provided in Fig. 3.
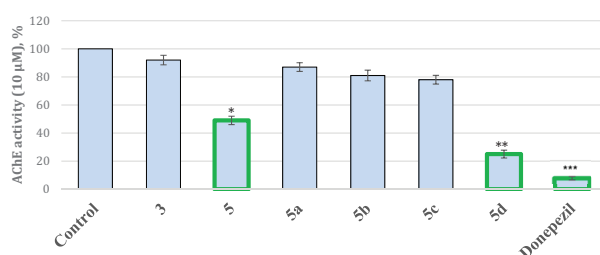

Figure 3. Activities of the title compounds against AChE applied as 10 μM concentrations. Data are presented as means from three independent experiments ± SD. * $P < 0.1$, ** $P < 0.01$, *** $P < 0.001$ vs control (pure eeAChE).

The most active compound was the hydrazide-hydrazone – 5d, with 75% inhibitory activity against the AChE enzyme. The unsubstituted hydrazide – 5, showed a good blocking ability of 51%. Interestingly, the pyrrole-based compounds substituted with 4-methoxy (5a), 2,4-dimethoxy (5b), and 2,3-dimethoxy (5c) benzaldehydes revealed no significant effects (13%, 19%, and 22%,

respectively). The initial pyrrole-carboxylic acid (3) was inactive against AChE. The results determined the importance of -OH in the benzene ring for significantly higher AChE activity.

Overall, it was noted that the most prominent dual acting MAO-B/AChE inhibitor is the hydrazide 5. The former compound exerted good MAO-B inhibitory activity (30% at 1 μM concentration) and excellent AChE blocking capacity (51% at 10 μM concentration).

Molecular docking in MAO-B

In an attempt to gain further understanding of the *in vitro* results, and to obtain additional insights into the active binding conformations of the inhibitors, molecular docking simulations of the title compounds within the active site of MAO-B (PDB: 2V5Z) and AChE (PDB: 4EY6) were carried out.

Initially, the docking simulations in MAO-B with GOLD 5.3 (ChemPLP scoring function) were performed. All ligands were successfully situated in the active site, however, only compounds 3 and 5 showed good theoretical results. Interestingly, Glide did not return any poses of the pyrrole-based ligands. Therefore, we included IFD calculations, which achieved good scores for compounds 3 and 5 (-11.20 kcal/mol, and -14.80 kcal/mol, respectively) (Table 2).

The GOLD's ChemPLP scoring algorithm obtained acceptable results for the N-pyrrolylcarboxilic acid 3 and the hydrazide 5. The substituted hydrazide-hydrazones demonstrated many steric clashes, which led to drastically lowered fitness scores. The docking calculations concluded that the IFD protocol is the most suitable considering the positive correlations with the *in vitro* data. The former

simulations did not acquire any results for 5a, 5b, 5c and 5d due to the inability of IFD to situate the ligands in the active site of MAO-B. Thus, the stabilizing intermolecular interactions were provided only for 3, 5 and the standards Safinamide and Selegiline (Table 3).

The active cavity of MAO-B is constructed of a substrate cavity and an entrance cavity. Furthermore, the substrate cavity includes an aromatic cage, which is of great importance for the MAO-B activity (Dasgupta et al. 2021). The active amino residues Ile199, Tyr326, Tyr398 and Tyr435 have been reported as essential for the selectivity against the B isoform (Tzvetkov et al. 2014). The N-pyrrolylcarboxylic acid (3), formed four π–π interactions with Tyr326, Tyr398 and Tyr435. The fragments, which participate in the former stable bonds, were the pyrrole and tryptophan aromatics. No hydrogen bond between 3 and MAO-B was formed. Importantly, the amino acids from the "aromatic cage" of the active site of MAO-B were included in the stabilizations of both 3 and 5. The visualization of the complex 5-MAO/B is provided in Fig. 4.

The tryptophan moiety of the hydrazide 5 was situated in the "aromatic cage" of the active site where it was stabilized by π–π interactions with Tyr398 and Tyr435. The former stabilizing interactions are important for the selective MAO-B activity. The pyrrole moiety was located in the substrate cavity of the enzyme, where Cys172, Ile198, Ile199, and Try326 were involved in π–π interactions with the aromatic heterocycle. The ethyl ester of 5 was placed in the entrance cavity. Importantly, the hydrazide was further stabilized by H-bond with the active amino acid Gln206. A stable H-bond was not present in the case of the N-pyrrolylcarboxilic acid 3 which could explain the enhanced experimental MAO-B inhibitory activity of 5.

Overall, the docking simulations in MAO-B demonstrated that shorter pyrrole-based compounds exert better MAO-B blocking capacities.

Molecular docking in AChE

Both GOLD 5.3 and Glide successfully returned active poses of all ligands when docked in AChE (PDB: 4EY6). The docking scores are presented in Table 4.

The most prominent AChE inhibitor from the *in vitro* studies – 5d (75% activity at 10 μM) revealed the best XP score of -14.27 kcal/mol and moderate ChemPLP score of 96.40. The most unfavorable scores were retrieved after

Table 2. GOLD 5.3 (ChemPLP) and IFD (XP score) docking scores after simulations in the active site of MAO-B (PDB: 2V5Z).

Compound	GOLD 5.3 (ChemPLP)	IFD (XP score)
3	113.16	-11.20
5	119.54	-14.80
5a	62.09	–
5b	42.98	–
5c	47.16	–
5d	42.35	–
*Safinamide	157.91	-15.83
*Selegiline	133.42	-8.54

*Reference drugs.

Table 3. Intermolecular stabilizations of the title compounds in MAO-B (PDB: 2V5Z).

| Compound	H-bonds	π–π bonds	Hydrophobic interactions
3	–	Tyr326 (4.78 Å), Tyr398 (3.58 Å, 4.33 Å), Tyr435 (4.17 Å)	Tyr60, Trp119, Leu167, Phe168, Leu171, Cys172, Tyr188, Ile198, Ile199, Leu328, Phe343
5	Gln206 (1.55 Å)	Tyr326 (4.88 Å), Tyr398 (3.71 Å, 4.00 Å), Tyr435 (4.22 Å)	Tyr60, Trp119, Leu167, Phe168, Leu171, Cys172, Tyr188, Ile198, Ile199, Ile316 Leu328, Phe343, Trp432
*Safinamide	Gln206 (1.87 Å, 1.97 Å), H_2O (1.61 Å)	Tyr326 (5.52 Å)	Tyr60, Trp119, Leu167, Phe168, Leu171, Cys172, Tyr188, Ile198, Ile199, Leu328, Phe343, Tyr398, Tyr435
*Selegiline	His115 (1.84 Å)	–	Phe103, Pro104, His115, Phe118, Trp119, Ala161, Leu164, Ala165, Leu167, Phe168, Leu171, Ile199

* Reference drugs.
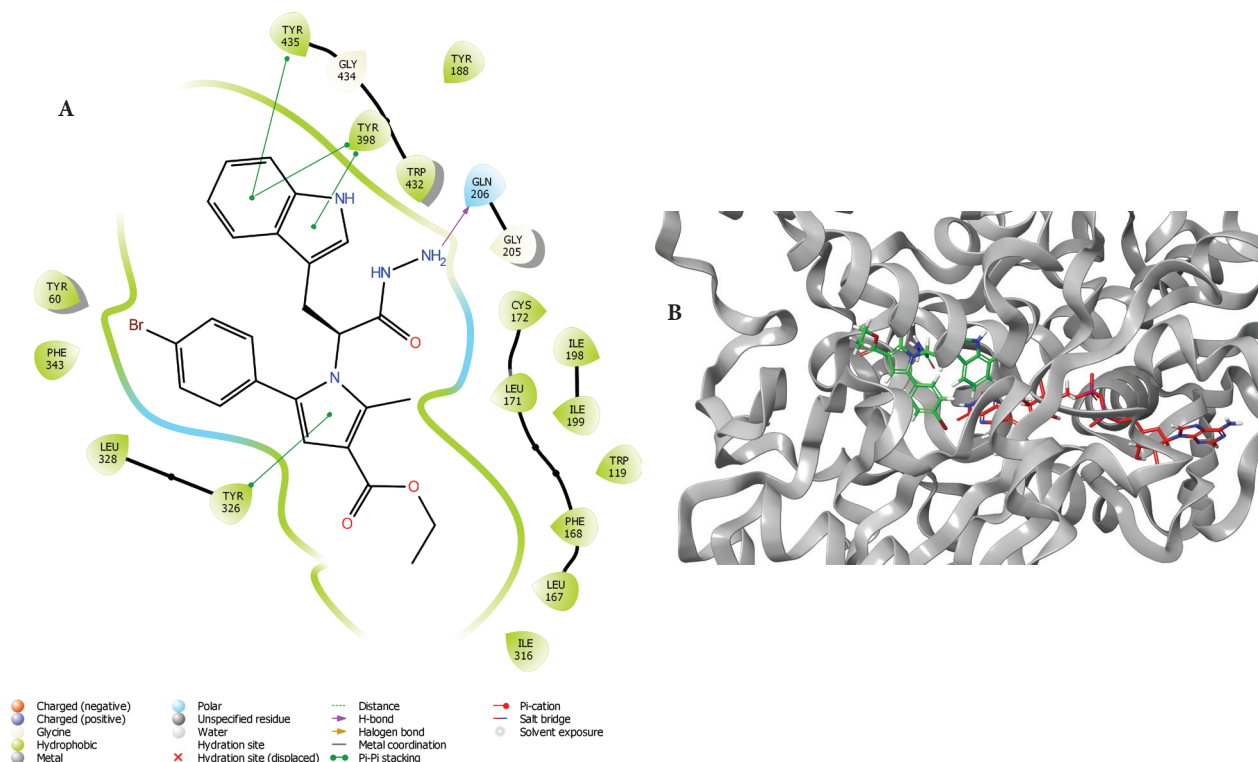
Figure 4. Visualizations of the intermolecular interactions of 5 with the active site of MAO-B (PDB: 2V5Z). **A.** 2D panel; **B.** 3D panel.

Table 4. GOLD 5.3 (ChemPLP) and Glide (XP score) docking scores after simulations in the active site of AChE (PDB: 4EY6).

Compunds	GOLD 5.3 (ChemPLP)	Glide (XP score)
3	83.75	-4.71
5	99.10	-10.28
5a	103.81	-12.19
5b	93.62	-13.04
5c	94.69	-12.68
5d	96.40	-14.27
*Galantamine	121.20	-9.47
*Donepezil	111.06	-18.72

*Reference drugs.

docking simulations with the N-pyrrolylcarboxilic acid 3. The former calculations were in good agreement with the experimental results. Interestingly, the highest GOLD 5.3 fitness scores was achieved by the hydrazide-hydrazone condensed with anisaldehyde - 5a (103.81). However, the *in vitro* data showed insignificant AChE inhibitory activity – 13% (10 μM). The former data illustrated the major disadvantage of the docking programs – increased risk for false-active ligands (Makeneni et al. 2018). The active amino acids involved in hydrogen bonds, π–π and hydrophobic interactions are provided in Table 5.

Importantly, most of the stabilizing interactions were with hydrophobic nature. The former bonds have been described in the stabilization of several active AChE inhibitors (Chigupati et al. 2016; Tang et al. 2019). The active amino acid Trp86 was involved in π–π bonds with most of the title pyrrole-based ligands. The significance of Trp86 for the formation of potent inhibitors is discussed by several research groups (Ordentlich et al. 1995; Ranjan et al. 2018).

Subsequent visualization of the intermolecular interactions between the most prominent dual inhibitor - 5, and the active site of AChE is given in Fig. 5.

The pyrrole-based hydrazide 5 formed compact active conformation in the active site of AChE. The tryptophan moiety was facing the entrance cavity of the enzyme, while the pyrrole fragment was situated in the substrate pocket. Additionally, a hydrogen bond between the active amino acid His447 and the secondary amino group stabilized the complex. Interestingly, the hydrazide 5 did not participate in any stabilizations with amino acids from the peripheral active site (PAS) which negatively affects the docking scores.

DFT calculations

A search for the most energetically favorable geometry of a ligand is fundamental prior to subsequent computational simulations. Therefore, the most prominent dual MAO-B/AChE inhibitor (5) was applied for full optimization calculations. Initial conformational search was performed by 250 iterations with OPLS4 force field. The energetically favorable conformations were further optimized by full DFT geometry optimization at B3LYP/6-311^{++} (d,p) level of theory. The most favorable conformation is given in Fig. 6.

Frontier molecular orbitals and global reactivity descriptors

A conceptual DFT analysis of the stability and reactivity of the most active dual inhibitor 5 was conducted by calculations of the highest occupied molecular orbital (HOMO),
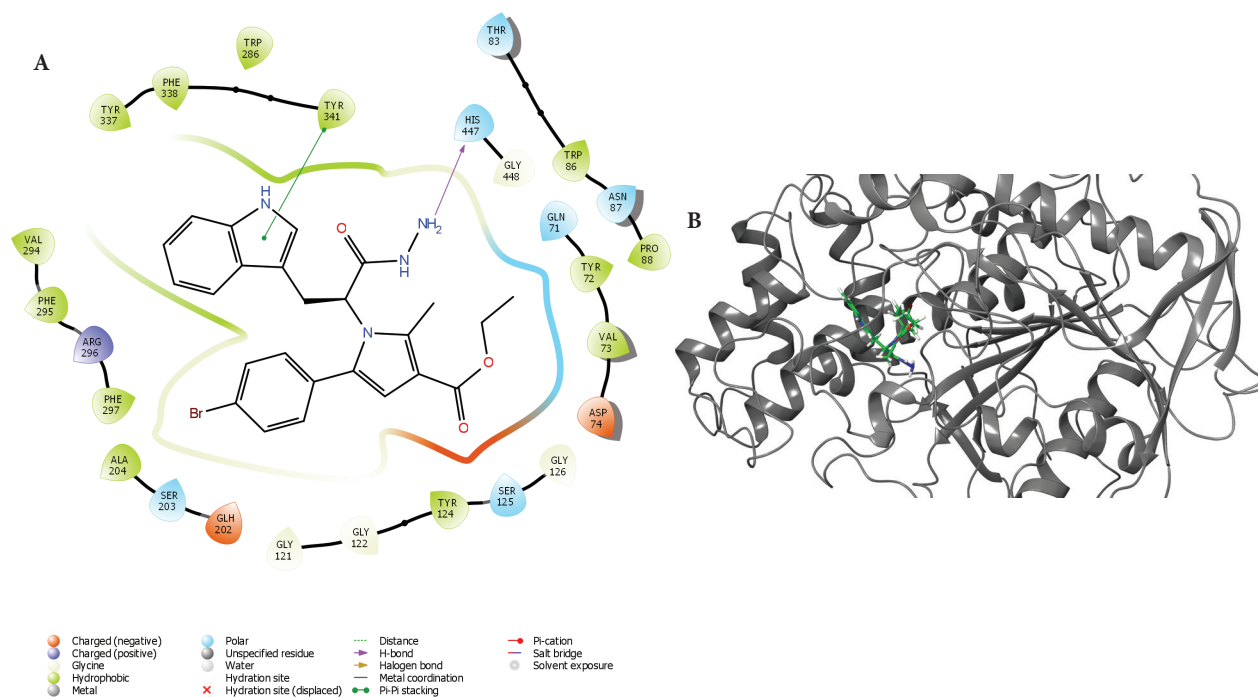
Figure 5. Major intermolecular interactions between the active site of 4EY6 and 5. **A.** 2D visualization; **B.** 3D visualization.

Table 5. Intermolecular stabilizations of the title compounds in AChE (PDB: 4EY6).

Compound	H-bonds	π–π bonds	Hydrophobic interactions
3	–	His447 (4.93 Å)	Tyr72, Val73, Trp86, Pro88, Tyr124, Tyr133, Ala204, Val294, Phe295, Tyr337, Phe338, Tyr341
5	His447 (2.46 Å)	Tyr341 (3.73 Å)	Tyr72, Val73, Trp86, Pro88, Tyr124, Tyr133, Ala204, Val294, Phe295, Phe297, Tyr337, Phe338, Tyr341
5a	H_2O (2.28 Å)	Trp286 (4.16 Å), Trp86 (3.52 Å, 3.95 Å, 4.34 Å)	Tyr72, Val73, Trp86, Pro88, Tyr124, Tyr133, Ala204, Val294, Phe295, Phe297, Tyr337, Phe338, Tyr341
5b	–	Trp286 (4.00 Å), Trp86 (3.54 Å, 3.97 Å, 4.35 Å)	Tyr72, Val73, Trp86, Pro88, Tyr124, Tyr133, Ala204, Val294, Phe295, Phe297, Tyr337, Phe338, Tyr341, Ile451
5c	–	Tyr341 (4.38 Å), Trp286 (4.08 Å), Trp86 (3.60 Å, 3.72 Å, 4.30 Å)	Tyr72, Val73, Trp86, Pro88, Tyr124, Tyr133, Ala204, Val294, Phe295, Phe297, Tyr337, Phe338, Tyr341, Ile451
5d	Tyr124 (2.2 Å), H_2O (1.96 Å)	Trp286 (3.96 Å), Trp86 (3.47 Å, 4.14 Å, 4.15 Å, 4.34 Å)	Tyr72, Val73, Trp86, Pro88, Tyr124, Tyr133, Ala204, Val294, Phe295, Phe297, Tyr337, Phe338, Tyr341, Ile451
TZ4	–	Trp86 (3.98 Å), Trp286 (6.15 Å, 6.17 Å)	Tyr72, Leu76, Trp86, Pro88, Tyr124, Tyr133, Trp286, Leu289, Phe295, Phe297, Tyr337, Tyr338, Tyr341, Ile451
*Donepezil	H_2O (1.81 Å), Phe295 (1.98 Å)	Trp86 (4.15 Å), Tyr337 (3.73 Å), Phe338 (6.07 Å)	Tyr72, Trp86, Tyr124, Tyr133, Trp286, Leu289, Val294, Phe295, Phe297, Tyr337, Tyr338, Tyr341
*Galantamine			

*Reference drugs.

the lowest unoccupied molecular orbital (LUMO). Subsequently, the values of the global reactivity descriptors, such as ionization potential (IP), electron affinity (EA), molecular hardness and softness, electronegativity and electrophilicity were obtained. The HOMO and LUMO electronic densities of 5 with DFT/B3LYP/6-311++(d,p) based calculations are given in Fig. 7. The positive phase was colored in blue, while the negative one in red.

It was found that the HOMO of 5 is mainly localized on the tryptophan moiety while the LUMO is centered around the p-bromophenyl fragment. Subsequently, the energies (in atomic units) of the FMOs and the global reactivity descriptors (hardness (η), softness (S), electronegativity (χ), chemical potential (μ), and electrophilicity index (ω)) were calculated by employing the Koopman's theorem (Tsuneda et al. 2010). The DFT calculations of

FMOs and global reactivity descriptors (in eV) are provided in Table 6.

The energies of HOMO and LUMO of one compound provide data about the distribution of the internal energy in a system. The ionization potential of compound 5 was significantly higher (5.5 eV) compared to the electron affinity value (0.86 eV). Therefore, the electron donor capacity of the pyrrole-based hydrazide is drastically enhanced than the electron donor ability. The big gap between the energies of the LUMO and HOMO represents the hydrazide 5 as a molecule with low polarity, low reactivity and high stability (Tawari et al. 2010). The global hardness η can be regarded as a direct measure of the electron density deformation and of the chemical reactivity. The η value of 5 (2.30 eV) revealed low reactivity (Pradeep et al. 2021). The negative value of the chemical potential (-3.16 eV) of compound 5 establishes
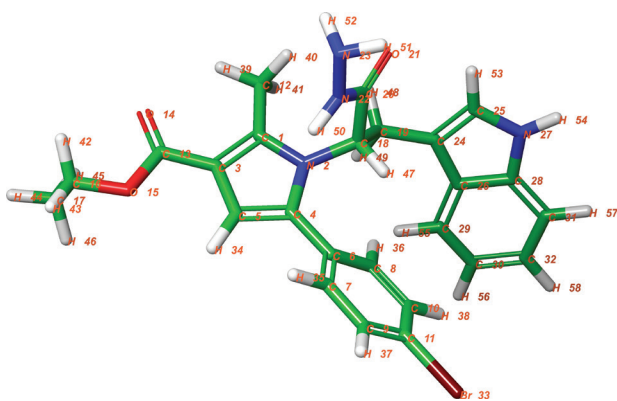
Figure 6. Optimized geometry of the most effective dual MAO-B/AChE inhibitor 5 at B3LYP/6-311++(d, p).

Table 6. FMOs energies and global reactivity descriptors for the dual inhibitor **5** at B3LYP/6-311++(d,p) level of theory.

Electronic parameter	5
E_{HOMO}	-5.508 eV
E_{LUMO}	-0.864 eV
$\Delta E_{HOMO-LUMO}$	4.644 eV
Ionization Energy (IP)	5.5 eV
Electron Affinity	0.86 eV
Chemical Hardness	2.30 eV
Softness	0.22 eV
Electronegativity	3.16 eV
Chemical Potential	-3.16 eV
Electrophilicity index	2.17 eV

Figure 7. HOMO (**A**) и LUMO (**B**) of the best dual acting MAO-B/AChE inhibitor – 5.

good stabilities, and resistance to sudden decomposition. The calculated electrophilicity index value (2.17 eV) is related to the chemical potential and hardness, and it is an indicator for the nucleophilicity power (Choudhary et al. 2019). The discussed DFT results showed that the best dual acting MAO-B/AChE inhibitor - 5, possess high ionization potential and low electron affinity. The noted big HOMO-LUMO gap represents the hydrazide as a stable molecule with low reactivity.

Conclusion

The conducted *in vitro* experiments revealed that the unsubstituted hydrazide 5 is the most promising dual acting MAO-B/AChE inhibitor in the series. Moreover, stable complexes were formed when 5 was docked into the active gorges of the crystallographic MAO-B and AChE struc-

tures. The molecular docking simulations revealed that the unsubstituted hydrazine moiety forms stable hydrogen bonds in both MAO-B and AChE enzymes. The importance of the tryptophan moiety was also noticed. The DFT calculations demonstrated that 5 is a stable molecule with low polarity and high electron donor capacity. Overall, a pyrrole-based compound was found as a dual-acting AchE/MAO-B inhibitor with good reported antioxidant properties. The latter could be considered as a candidate for future lead-optimizations.

Acknowledgments

References

Altintop MD, Sever B, Osmaniye D, Sağlık BN, Özdemir A (2018) Design, synthesis, *in vitro* and *in silico* evaluation of new pyrrole derivatives as monoamine oxidase inhibitors. Archiv der Pharmazie 351: 1800082. https://doi.org/10.1002/ardp.201800082

Bochevarov AD, Harder E, Hughes TF, Greenwood JR, Braden DA, Philipp DM, Rinaldo D, Halls MD, Zhang J, Friesner RA (2013) Jaguar: A high-performance quantum chemistry software program with strengths in life and materials sciences. International Journal of Quantum Chemistry 113: 2110–2142. https://doi.org/10.1002/qua.24481
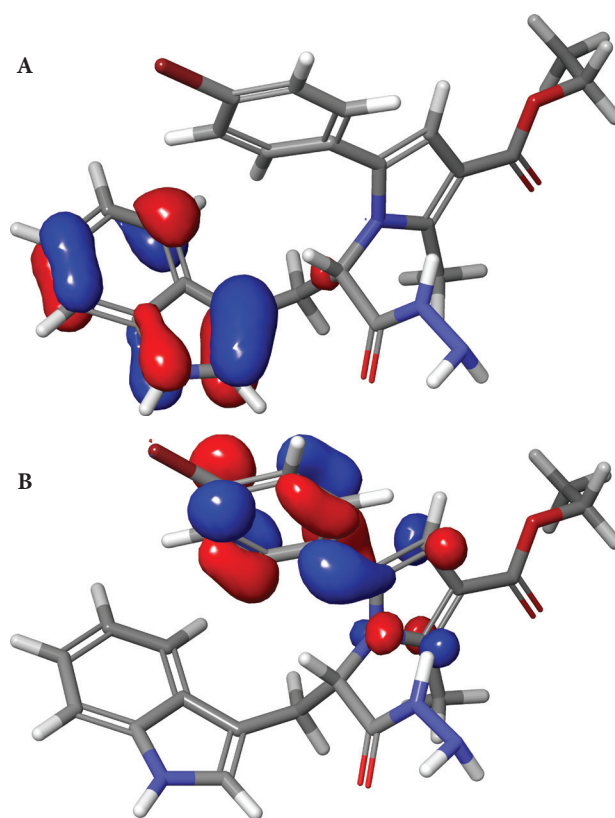
Chigurupati S, Selvaraj M, Mani V, Selvarajan KK, Mohammad JI, Kaveti B, Bera H, Palanimuthu VR, Teh LK, Salleh MZ (2016) Identification of novel acetylcholinesterase inhibitors: Indolopyrazoline derivatives and molecular docking studies. Bioorganic Chemistry 67: 9–17. https://doi.org/10.1016/j.bioorg.2016.05.002

Choudhary V, Bhatt A, Dash D, Sharma N (2019) DFT calculations on molecular structures, HOMO–LUMO study, reactivity descriptors and spectral analyses of newly synthesized diorganotin(IV) 2-chloridophenylacetohydroxamate complexes.

Journal of Computational Chemistry 40: 2354–2363. https://doi.org/10.1002/jcc.26012

Dasgupta S, Mukherjee S, Sekar K, Mukhopadhyay BP (2020) The conformational dynamics of wing gates Ile199 and Phe103 on the binding of dopamine and benzylamine substrates in human monoamine Oxidase B. Journal of Biomolecular Structure and Dynamics 39: 1879–1886. https://doi.org/10.1080/07391102.2020.1734483

Galimberti D, Scarpini E (2016) Old and new acetylcholinesterase inhibitors for Alzheimer's disease. Expert Opinion on Investigational Drugs 25: 1181–1187. https://doi.org/10.1080/13543784.2016.1216972

González JF, Alcántara AR, Doadrio AL, Sánchez-Montero JM (2019) Developments with multi-target drugs for Alzheimer's disease: an overview of the current discovery approaches. Expert Opinion on Drug Discovery 14: 879–891. https://doi.org/10.1080/17460441.2019.1623201

Huang L-K, Chao S-P, Hu C-J (2020) Clinical trials of new drugs for Alzheimer disease. Journal of biomedical science 27: 18. https://doi.org/10.1186/s12929-019-0609-7

Karlawish J, Grill JD (2021) The approval of Aduhelm risks eroding public trust in Alzheimer research and the FDA. Nature Reviews Neurology 17: 523–524. https://doi.org/10.1038/s41582-021-00540-6

Makeneni S, Thieker DF, Woods RJ (2018) Applying pose clustering and MD simulations to eliminate false positives in molecular docking. Journal of Chemical Information and Modeling 58: 605–614. https://doi.org/10.1021/acs.jcim.7b00588

Mateev E (2022) Design, synthesis, biological evaluation and molecular docking of pyrrole-based compounds as antioxidant and MAO-b inhibitory agents. Farmacia 70: 344–354. https://doi.org/10.31925/farmacia.2022.2.21

Mateev E, Georgieva M, Zlatkov A (2022a) Design, microwave-assisted synthesis, biological evaluation, molecular docking and ADME studies of pyrrole-based hydrazide-hydrazones as potential antioxidant agents. Macedonian Journal of Chemistry and Chemical Engineering 41(2): 175–186. https://doi.org/10.20450/mjcce.2022.2494

Mateev E, Georgieva M, Zlatkov A (2022b) Pyrrole as an important scaffold of anticancer drugs: Recent advances. Journal of Pharmacy and Pharmaceutical Sciences 25: 24–40. https://doi.org/10.18433/jpps32417

Mateeva A, Peikova L, Kondeva-Burdina M, Georgieva M (2022) Development of new HPLC method for identification of metabolic degradation of N-pyrrolylhydrazide hydrazones with determined MAO-B activity in cellular cultures. Pharmacia 69: 15–20. https://doi.org/10.3897/pharmacia.69.e78417

Mathew B, Parambi DGT, Mathew GE, Uddin MS, Inasu ST, Kim H, Marathakam A, Unnikrishnan MK, Carradori S (2019) Emerging therapeutic potentials of dual-acting MAO and AChE inhibitors in Alzheimer's and Parkinson's diseases. Archiv der Pharmazie 352: 1900177. https://doi.org/10.1002/ardp.201900177

Mohsen U, KocyigitKaymakcioglu B, OrucEmre E, Kaplancikli Z, Rollas S (2015) Studies on hydrazide-hydrazon derivatives as acetylcholinesterase inhibitors. Journal of Marmara University Institute of Health Sciences: 1(1): 10–14. https://doi.org/10.5455/musbed.20141117035707

Ordentlich A, Barak D, Kronman C, Ariel N, Segall Y, Velan B, Shafferman A (1995) Contribution of aromatic moieties of Tyrosine 133 and of the anionic subsite Tryptophan 86 to catalytic efficiency and allosteric modulation of acetylcholinesterase. Journal of Biological Chemistry 270: 2082–2091. https://doi.org/10.1074/jbc.270.5.2082

Popiołek Ł (2021) The bioactivity of benzenesulfonyl hydrazones: A short review. Biomedicine and Pharmacotherapy 141: 111851. https://doi.org/10.1016/j.biopha.2021.111851

Pradeep S, Jain AS, Dharmashekara C, Prasad SK, Akshatha N, Pruthvish R, Amachawadi RG, Srinivasa C, Syed A, Elgorban AM, Al Kheraif AA, Ortega-Castro J, Frau J, Flores-Holguín N, Shivamallu C, Kollur SP, Glossman-Mitnik D (2021) Synthesis, computational pharmacokinetics report, conceptual DFT-based calculations and anti-acetylcholinesterase activity of hydroxyapatite nanoparticles derived from *Acorus calamus* plant extract. Frontiers in Chemistry 9: 741037-741037. https://doi.org/10.3389/fchem.2021.741037

Raina P, Santaguida P, Ismaila A, Patterson C, Cowan D, Levine M, Booker L, Oremus M (2008) Effectiveness of cholinesterase inhibitors and memantine for treating dementia: Evidence review for a clinical practice guideline. Annals of Internal Medicine 148: 379. https://doi.org/10.7326/0003-4819-148-5-200803040-00009

Raka SC, Ahamed R, Rahman A, Momen AZMR (2019) *In silico* discovery of noteworthy multi-targeted acetylcholinesterase inhibitors for the treatment of Alzheimer's disease. Advances in Traditional Medicine 20: 351–366. https://doi.org/10.1007/s13596-019-00407-8

Ranjan A, Chauhan A, Jindal T (2018) *In-silico* and *in-vitro* evaluation of human acetylcholinesterase inhibition by organophosphates. Environmental Toxicology and Pharmacology 57: 131–140. https://doi.org/10.1016/j.etap.2017.12.014

Sang Z, Song Q, Cao Z, Deng Y, Zhang L (2022) Design, synthesis, and evaluation of chalcone-Vitamin E-donepezil hybrids as multi-target-directed ligands for the treatment of Alzheimer's disease. Journal of Enzyme Inhibition and Medicinal Chemistry 37: 69–85. https://doi.org/10.1080/14756366.2021.1993845

Schedin-Weiss S, Inoue M, Hromadkova L, Teranishi Y, Yamamoto NG, Wiehager B, Bogdanovic N, Winblad B, Sandebring-Matton A, Frykman S, Tjernberg LO (2017) Monoamine oxidase B is elevated in Alzheimer disease neurons, is associated with γ-secretase and regulates neuronal amyloid β-peptide levels. Alzheimer's Research & Therapy 9: 57. https://doi.org/10.1186/s13195-017-0279-1

Sitaram N, Weingartner H, Caine ED, Christian Gillin J (1978) Choline: Selective enhancement of serial learning and encoding of low imagery words in man. Life Sciences 22: 1555–1560. https://doi.org/10.1016/0024-3205(78)90011-5

Tang H, Song P, Li J, Zhao D (2019) Effect of *Salvia miltiorrhiza* on acetylcholinesterase: Enzyme kinetics and interaction mechanism merging with molecular docking analysis. International Journal of Biological Macromolecules 135: 303–313. https://doi.org/10.1016/j.ijbiomac.2019.05.132

Tanzi RE (2021) FDA Approval of Aduhelm Paves a New Path for Alzheimer's Disease. ACS Chemical Neuroscience 12: 2714–2715. https://doi.org/10.1021/acschemneuro.1c00394

Tawari NR, Bairwa R, Ray MK, Rajan MGR, Degani MS (2010) Design, synthesis, and biological evaluation of 4-(5-nitrofuran-2-yl) prop-2-en-1-one derivatives as potent antitubercular agents. Bioorganic & Medicinal Chemistry Letters 20: 6175–6178. https://doi.org/10.1016/j.bmcl.2010.08.127

Tsuneda T, Song J-W, Suzuki S, Hirao K (2010) On Koopmans' theorem in density functional theory. The Journal of Chemical Physics 133: 174101. https://doi.org/10.1063/1.3491272

Tzvetkov NT, Hinz S, Küppers P, Gastreich M, Müller CE (2014) Indazole- and Indole-5-carboxamides: Selective and Reversible Monoamine Oxidase B Inhibitors with Subnanomolar Potency. Journal of Medicinal Chemistry 57: 6679–6703. https://doi.org/10.1021/jm500729a